UV GAS LASER INVESTIGATIONS

M. L. Bhaumik, et al

Northrop Research and Technology Center

Prepared for:

Office of Naval Research
Advanced Research Projects Agency

November 1974

UNCLASSIFIED

SECURITY CLASSIFICATION OF THIS PAGE (When Data Entered)

AD/A002 477

REPORT DOCUMENTATION PAGE

READ INSTRUCTIONS BEFORE COMPLETING FORM

1. REPORT NUMBER: NRTC 74-70R	2. GOVT ACCESSION NO.
3. RECIPIENT'S CATALOG NUMBER	
4. TITLE (and Subtitle): UV Gas Laser Investigations	5. TYPE OF REPORT & PERIOD COVERED: Semiannual Technical Report
6. PERFORMING ORG. REPORT NUMBER: NRTC 74-70R	
7. AUTHOR(s): M. L. Bhaumik and E. R. Ault	8. CONTRACT OR GRANT NUMBER(s): N00014-72-C-0456
9. PERFORMING ORGANIZATION NAME AND ADDRESS: Northrop Research and Technology Center, 3401 West Broadway, Hawthorne, California 90250	10. PROGRAM ELEMENT, PROJECT, TASK AREA & WORK UNIT NUMBERS: ARPA Order No. 1807
11. CONTROLLING OFFICE NAME AND ADDRESS: Advanced Research Projects Agency, 1400 Wilson Blvd., Arlington, Virginia 22209	12. REPORT DATE: November 1974
	13. NUMBER OF PAGES: 36
14. MONITORING AGENCY NAME & ADDRESS (if different from Controlling Office): Office of Naval Research, Department of the Navy, Arlington, Virginia 22217	15. SECURITY CLASS. (of this report): Unclassified
	15a. DECLASSIFICATION/DOWNGRADING SCHEDULE: -

16. DISTRIBUTION STATEMENT (of this Report)

None

17. DISTRIBUTION STATEMENT (of the abstract entered in Block 20, if different from Report)

None

18. SUPPLEMENTARY NOTES

None

19. KEY WORDS (Continue on reverse side if necessary and identify by block number)

Laser Oscillations
Ar-N_2
Transfer Lasers
Ultraviolet Lasers

20. ABSTRACT (Continue on reverse side if necessary and identify by block number)

The results of an intensive study of the high power characteristics of the Ar-N_2 laser are described. A kinetic model predicting efficiencies as high as 4% is developed and contrasted to a series of experiments carried out concurrent with the calculations. Laser energies as high as 0.23J at powers of 10 MW have been obtained with the Pulserad 535, a 3 MeV, 60 kA, 50 ns electron gun supplied by DNA. This output was obtained at an estimated efficiency of 2%. The laser oscillates on 2 lines, 3577Å and 3805Å, sequentially. The implications of this observation are discussed.

DD FORM 1 JAN 73 1473 EDITION OF 1 NOV 65 IS OBSOLETE

UNCLASSIFIED

SECURITY CLASSIFICATION OF THIS PAGE (When Data Entered)

NRTC 74-70R

UV GAS LASER INVESTIGATIONS
SEMIANNUAL TECHNICAL REPORT

November 1974

Prepared by

M. L. Bhaumik and E. R. Ault

Contract N00014-72-C-0456

Sponsored by

ADVANCED RESEARCH PROJECTS AGENCY
ARPA Order No. 1807

Monitored by

OFFICE OF NAVAL RESEARCH
Code 421

NORTHROP CORPORATION
Northrop Research and Technology Center
Short Wavelength Laser Programs
3401 West Broadway
Hawthorne, California 90250
(213) 675-4611, Ext. 4756

UV GAS LASER INVESTIGATIONS

ARPA Order Number:	1807
Program Code Number:	5E20
Contract Number:	N00014-72-C-0456
Principal Investigator and Telephone Number:	Dr. M. L. Bhaumik (213) 675-4611, Ext. 4756
Name of Contractor:	Northrop Corporation Northrop Research and Technology Center
Scientific Officer:	Director, Physics Programs Physical Sciences Division Office of Naval Research Department of the Navy 800 North Quincy Street Arlington, Virginia 22217
Effective Date of Contract:	15 April 1972 to 30 June 1975
Amount of Contract:	$652,500.00
Sponsored by:	Advanced Research Projects Agency ARPA Order No. 1807

TABLE OF CONTENTS

1.0 SUMMARY

The overall objective of this program is the development of new, visible and sl orter wavelength lasers capable of high power operation with high efficiency. The specific objective for this reporting period has been to carry out analytical and experimental investigations to obtain a better understanding of the newly discovered Ar-N_2 excitation transfer laser, leading to an optimization of power and efficiency. Working toward these objectives, the following key results were obtained:

(1) Kinetic modeling studies of the Ar-N_2 system were carried out with a CDC 6600 computer to determine the transient population densities. These studies indicate that high intracavity powers are essential for efficient operation of the Ar-N_2 laser because it is necessary to have a high rate of energy extraction by stimulated emission to compete successfully with nonradiative losses from the upper laser state. The modeling studies further indicate that efficiencies as high as 4% may be achieved with an Ar-N_2 laser.

(2) Experiments carried out with the Pulserad 535 excitation facility, which delivers a 3 MeV, 60 kA, 60 ns E-beam, gave the highest laser efficiency achieved so far in the near UV region. Typically, a peak power of several megawatts was obtained in a 40 ns pulse (FWHM) with an efficiency of $\sim$2%. This represents an order of magnitude improvement in efficiency for the Ar-N_2 laser over that reported previously. These results also seem to corroborate the analytical prediction that large intracavity powers are necessary to obtain a high extraction efficiency.

(3) The operation of the Ar-N_2 laser for 40 ns in a 12 cm long cavity represents 80 passes in the cavity, leaving little doubt that a true laser oscillator has been achieved. The results imply that relaxation of the laser terminal state must occur with rates comparable to that of the stimulated emission for intracavity powers in the MW

range. However, indications of laser saturation were obtained with higher intracavity powers. With powers in the range of 5 MW, the laser switched from the 0-1 to the 0-2 transition during the latter part of the pulse. Modulation of the laser pulse, indicative of relaxation oscillations, was also observed. Finally, at higher pressures the laser completely saturated giving only a high intensity short spike with intracavity powers in the range of tens of megawatts. Intensities for which saturation was experimentally observed were on the same order of magnitude as the saturation intensity estimated from theoretical analysis. The laser also seems to be more efficient when it operates in this high pressure, short spike mode. However, mirror damage at these high intensities has prevented an accurate measurement of the efficiency so far.

The details of these results are described in the following sections. First, the background of the Ar-N_2 laser is given in the Introduction. Then the details of the kinetic modeling and the analytical investigation are described. This is followed by the details of the experiments and results together with pertinent discussions. The newly completed Pulserad 535 excitation facility is also described in the experimental section.

2.0 INTRODUCTION

The achievement[1] of high efficiency vacuum ultraviolet excimer lasers has demonstrated the importance of rare gases for efficiently converting electrical energy into radiation at short wavelengths. Analytical investigations at Northrop and other laboratories indicate that due to uniquely favorable kinetic processes, the rare gas excimers may be capable of electrical conversion efficiencies up to 50%. However, the radiation from the rare gas excimers occurs only in the VUV region of the spectrum. Although high energy lasers in these wavelengths are important for some special applications, it would be more desirable to obtain high efficiency lasers in the transmissive region of the atmosphere, since that would lead to more versatile applications.

The high conversion efficiency of the rare gas excimers may be successfully employed to develop visible and near UV lasers by using suitable energy transfer schemes. In such a scheme, the rate of energy transfer to the acceptor molecule must be higher than the rate of energy losses in the rare gas itself. Furthermore, the branching ratio of the transferred energy to the various levels of the acceptor molecule must be favorable for a population inversion. If a donor-acceptor pair of this type is found, one that shows a high rate of energy transfer that very specifically populates the upper laser level, an efficiency of 10 to 20% may be realized near visible wavelengths. A block diagram of this scheme is shown in Figure 1.

The validity of this approach was demonstrated successfully at Northrop by the operation of a high power Ar-N_2 transfer laser at 3577Å. The pertinent energy level diagram of this system is shown in Figure 2. In this system, electrical energy absorbed by Ar is transferred to the N_2 molecule leading to laser oscillations on the transition $C^3\Pi_u \rightarrow B^3\Pi_g$. A peak laser power of 0.5 MW with an estimated efficiency of 0.2% was achieved by E-beam excitation of a mixture of 92 psia Ar and 8 psia N_2. The details

APPROACH

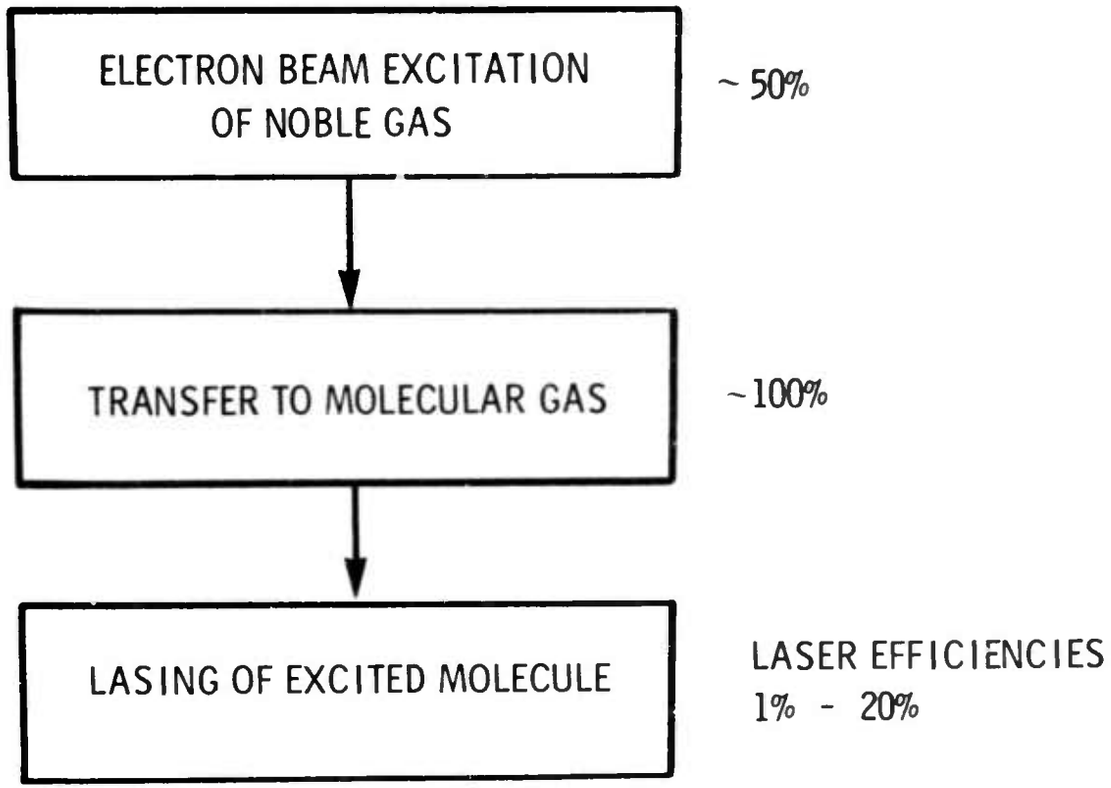

Figure 1. Block diagram showing our approach for developing a high efficiency laser near visible wavelengths.

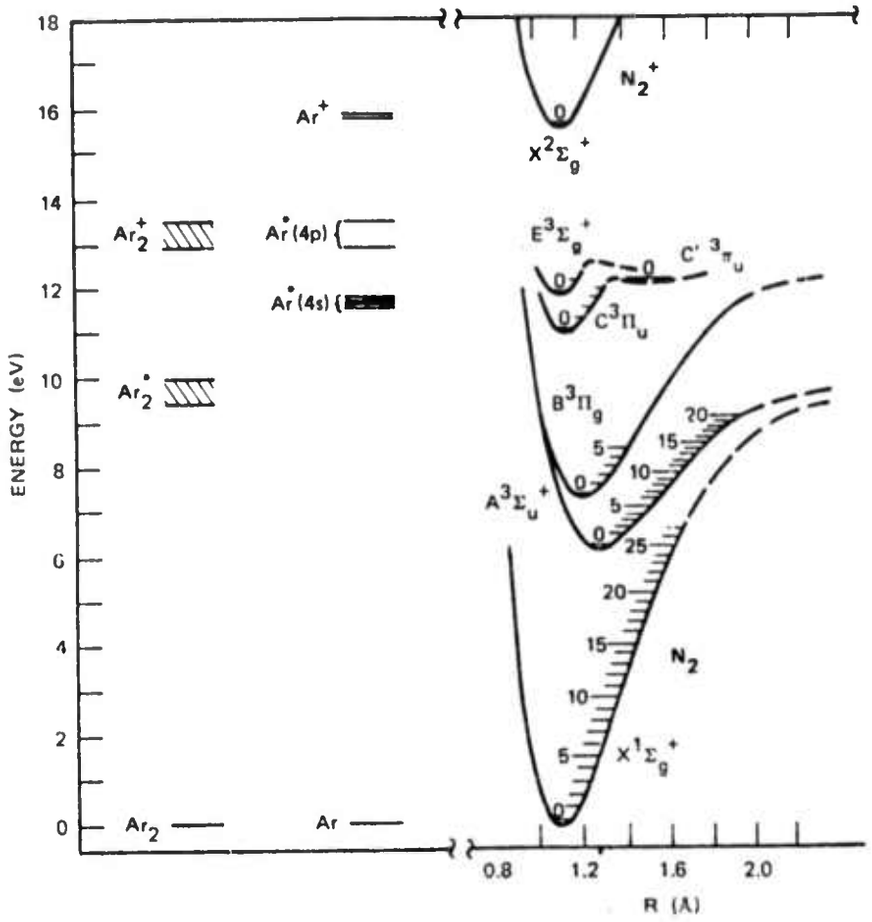

Figure 2. Pertinent energy level diagram of the Ar/N_2 system (from reference 2).

of these studies were described in the previous semiannual technical report, NRTC 74-26R.

The Ar-N_2 system deserves a thorough investigation in view of the initial spectacular success. Accordingly, a concerted effort has been devoted to the understanding of the laser mechanism by kinetic modeling and parametric investigations. Considering the energy balance of the various levels shown in the energy level diagram (Figure 2), the most likely energy donor appears to be the group of atomic argon metastable states designated by $Ar^*(4s)$. These metastable states are the predecessors of the argon excimers in the kinetic processes. For the present kinetic model, the argon metastables, rather than the excimers, have been considered as donors.

The experimental program includes the optimization of power and efficiency of the Ar-N_2 laser. A completely new E-beam excitation facility capable of delivering a 3 MeV, 60 kA, 60 ns E-beam, was used for this purpose. Progress of the program to date is described in the following sections.

3.0 KINETIC MODELING OF AR-N_2 LASER

The predominant mechanism by which energy from a high energy E-beam is absorbed by Ar is by ion-electron pair production. The relativistic (high energy) electron produces[3] 3.5 Ar^+ and 1 Ar^* by losing 91 eV. Any energy in excess of the ionization and atomic excitation energy appears as the energy of the secondary electrons. But the secondary electrons may be assumed to cool rapidly due to high rate of collisions in the high pressure gas; therefore pumping of Ar or N_2 by secondary electrons is not expected to make a significant contribution. The energy pumping by ion-electron pair production was introduced into the computer program in the form of a cross section using the following equation:

$$\frac{dn(Ar^+)}{dt} = \frac{J}{e} n(Ar)\, \sigma(+)$$

where $n(Ar^+)$ is the number density of Ar ions, J is the current density, e, the electronic charge, n(Ar) the number density of Ar atoms and $\sigma(+)$ is the cross section for producing Ar^+. A similar cross section $\sigma(*)$ was derived for the production of Ar^* by high energy electrons.

Since 3.5 Ar^+ and 1.0 Ar^* are produced for each 91 eV loss of E-beam energy,

$$\sigma(+)\, n(Ar) = 3.5 \frac{dE/dx}{91}$$

$$\sigma(*)\, n(Ar) = \frac{dE/dx}{91}$$

Taking dE/dx = 2.5 keV/cm at 1 atm of Ar (300°K), [4]

$$\sigma(+) = 3.85 \times 10^{-18}\ cm^2$$

$$\sigma(*) = 1.1 \times 10^{-18}$$

The rest of the analysis is rather straightforward even though the Ar excitation followed by energy transfer to N_2 and relaxation processes in

N_2 involves a large number of reactions. The task is, however, made difficult due to lack of accurate knowledge of the rate constants of some of the key reactions. In the present model, all the possible processes judged to be pertinent are included and are shown in Table I. The best available rate constants of these processes, taken from reference 2, are shown in Table II. The unknown rates or those which seem to be negligible are taken as 0 for the present.

The set of differential equations constructed to represent the processes shown in Table I together with their rate constants given in Table II were solved by using a CDC 6600 computer. A Runge-Kutta integration technique was used which resulted in the smallest integration time. In addition to the normal tabulation of the results, a plot routine was used to display a population density vs time plot. Figures 3, 4, and 5 show the population densities of the various species due to excitation of 4 atm Ar + 5% N_2 by a 1.5 kA, 2 ns E-beam. These plots are typical of a large number of plots representing various pressures, mixtures, and current densities. In all of these cases, the population density of $N_2(B)$, the lower laser level was higher. This is consistent with the experimental result that the laser does not operate on the $N_2(C)$ $v' = 0 \rightarrow N_2(B)$ $v'' = 0$. But $N_2(B)$ $v'' = 1$, situated 1734 cm^{-1} above the $v'' = 0$, has a population 2.7×10^{-4} that of $v'' = 0$. For the examples given here the peak population of $N_2(C)$ is 8×10^{14}/cc. The corresponding population of the $N_2(B)v'' = 0$ and $v'' = 1$ levels are 3×10^{15} and 10^{11}/cc, respectively. Therefore, the inversion between $N_2(C)$ $v' = 0$ and $N_2(B)$ v'' is obvious. Of course, an inversion also exists between $N_2(C)$ $v' = 0$ and still higher vibrational levels of $N_2(B)$.

The best means to test the validity of modeling is by comparing the above populatior with those derived from the measurement of small signal gain. Accordingly, an experimental arrangement is being completed for this purpose using the Pulserad 110A. Furthermore, a transient oscillator

Table I. Reactions Assumed in the Present Kinetic Model

REACTIONS INVOLVING EXCITATION AND KINETICS OF THE EXCITED AR SPECIES --

0) $AR(0) + HE(-) \rightarrow AR(+) + HE(-) + E(-)$
CURRENT = IBEAM, CROSS SECTION = SIGMA

1) $AR(0) + E(-) \rightarrow AR(+) + E(-)$

2) $AR(+) + AR(0) + AR \rightarrow AR2(+) + AR$

3) $AR(+) + AR(0) + N2 \rightarrow AR2(+) + N2$

4) $AR2(+) + E(-) \rightarrow AR(*) + AR(0)$

5) $AR(*) + AR(0) + AR \rightarrow AR2(*) + AR$

6) $AR(*) + AR(0) + N2 \rightarrow AR2(*) + N2$

7) $AR2(*) + E(-) \rightarrow AR(0) + AR(0) + E(-)$

8) $AR(*) + AR(*) \rightarrow AR(+) + AR(0) + E(-)$

9) $AR2(*) + AR2(*) \rightarrow AR2(+) + 2AR(0) + E(-)$

10) $AR2(*) \rightarrow AR(0) + AR(0) + HNU$

11) $AR(0) + E(-) \rightarrow AR(*) + E(-)$

12) $AR(*) + AR \rightarrow AR(0) + AR$

13) $AR(*) + N2 \rightarrow AR(0) + N2$

14) $AR(*) \rightarrow AR(0) + HNU$

Table I. Reactions Assumed in the Present Kinetic Model (continued)

REACTIONS INVOLVING EXCITATION AND KINETICS OF THE EXCITED N2 SPECIES --

15) $N2(X) + E(-) \rightarrow N2(A) + E(-)$

16) $N2(X) + E(-) \rightarrow N2(B) + E(-)$

17) $N2(X) + E(-) \rightarrow N2(C) + E(-)$

18) $N2(X) + E(-) \rightarrow N2(C1) + E(-)$

19) $N2(X) + E(-) \rightarrow N2(*) + E(-)$

20) $N2(A) + E(-) \rightarrow N2(B) + E(-)$

21) $N2(A) + E(-) \rightarrow N2(C) + E(-)$

22) $N2(B) + E(-) \rightarrow N2(C) + E(-)$

23,24) $N2(C1) + (AR,N2) \rightarrow N2(C) + (AR,N2)$

25,26) $N2(C1) + (AR,N2) \rightarrow N2(B) + (AR,N2)$

27,28) $N2(C1) + (AR,N2) \rightarrow N2(A) + (AR,N2)$

29,30) $N2(C1) + (AR,N2) \rightarrow N2(X) + (AR,N2)$

31,32) $N2(C) + (AR,N2) \rightarrow N2(B) + (AR,N2)$

33,34) $N2(C) + (AR,N2) \rightarrow N2(A) + (AR,N2)$

35,36) $N2(C) + (AR,N2) \rightarrow N2(X) + (AR,N2)$

37,38) $N2(B) + (AR,N2) \rightarrow N2(A) + (AR,N2)$

39,40) $N2(B) + (AR,N2) \rightarrow N2(X) + (AR,N2)$

41,42) $N2(A) + (AR,N2) \rightarrow N2(X) + (AR,N2)$

NEAR RESONANT (CROSS RELAXATION) PROCESSES AMONG THE EXCITED N2 STATES --

43) $N2(A) + N2(A) \rightarrow N2(C1) + N2(X)$

44) $N2(A) + N2(A) \rightarrow N2(C) + N2(X)$

45) $N2(B) + N2(B) \rightarrow N2(C) + N2(X)$

46) $N2(A) + N2(B) \rightarrow N2(C) + N2(X)$

47) $N2(A) + N2(C) \rightarrow N2(B) + N2(B)$

48) $N2(A) + N2(A) \rightarrow N2(B) + N2(X)$

Table I. Reactions Assumed in the Present Kinetic Model (continued)

SPONTANEOUS RADIATIVE DECAY PROCESSES FOR THE EXCITED N2 STATES--

49) $N_2(C) \rightarrow N_2(B) + h\nu$

50) $N_2(C) \rightarrow N_2(A) + h\nu$

51) $N_2(C) \rightarrow N_2(X) + h\nu$

52) $N_2(B) \rightarrow N_2(A) + h\nu$

53) $N_2(B) \rightarrow N_2(X) + h\nu$

54) $N_2(A) \rightarrow N_2(X) + h\nu$

RESONANT ENERGY EXCHANGE (CROSS-RELAXATION) REACTIONS --

55) $Ar(*) + N_2(X) \rightarrow Ar(0) + N_2(A)$

56) $Ar(*) + N_2(X) \rightarrow Ar(0) + N_2(B)$

57) $Ar(*) + N_2(X) \rightarrow Ar(0) + N_2(C)$

58) $Ar(*) + N_2(X) \rightarrow Ar(0) + N_2(C1)$

59) $Ar(*) + N_2(X) \rightarrow Ar(0) + N_2(*)$

60) $Ar_2(*) + N_2(X) \rightarrow 2Ar(0) + N_2(A)$

61) $Ar_2(*) + N_2(X) \rightarrow 2Ar(0) + N_2(B)$

62) $Ar_2(*) + N_2(X) \rightarrow 2Ar(0) + N_2(C)$

63) $Ar_2(*) + N_2(X) \rightarrow 2Ar(0) + N_2(C1)$

64) $Ar_2(*) + N_2(X) \rightarrow 2Ar(0) + N_2(*)$

MISCELLANEOUS REACTIONS WITH OTHER SPECIES --

65) $N_2(A) + NO(X) \rightarrow N_2(X) + NO(A)$

66,67) $NO(A) + (Ar, N_2) \rightarrow NO(X) + (Ar, N_2)$

68) $NO(A) \rightarrow NO(X) + h\nu$

Table II. Rate coefficient in cm^6/sec or cm^3/sec for the reactions given in Table I. KF(I) and KF(R) denote the rate of forward and backward reactions, respectively.

Reaction Number	KF(I)	KR(I)
1	0.	0.
2	2.5000E-31	0.
3	0.	0.
4	1.0000E-06	0.
5	1.0000E-32	0.
6	0.	0.
7	1.0000E-09	0.
8	5.0000E-10	0.
9	5.0000E-10	0.
10	2.4000E-07	0.
11	0.	0.
12	0.	0.
13	0.	0.
14	0.	0.
15	0.	0.
16	0.	0.
17	0.	0.
18	0.	0.
19	0.	0.
20	0.	0.
21	0.	0.
22	0.	0.
23	3.0000E-12	0.
24	0.	0.
25	0.	0.
26	0.	0.
27	0.	0.
28	0.	0.
29	0.	0.
30	0.	0.
31	8.0000E-13	0.
32	1.1000E-11	0.
33	0.	0.
34	0.	0.
35	0.	0.
36	0.	0.
37	1.0000E-14	0.
38	2.6000E-12	0.
39	0.	0.
40	0.	0.
41	0.	0.
42	0.	0.
43	1.0000E-11	0.
44	1.0000E-11	0.
45	1.0000E-13	0.
46	0.	0.
47	0.	0.
48	8.0000E-11	0.
49	2.2000E+07	0.
50	0.	0.
51	0.	0.
52	1.2000E+05	0.
53	0.	0.
54	0.	0.
55	0.	0.
56	1.7000E-11	0.
57	3.0000E-12	0.
58	1.0000E-11	0.
59	0.	0.
60	0.	0.
61	1.0000E-11	0.
62	0.	0.
63	0.	0.
64	0.	0.
65	8.0000E-11	0.
66	0.	0.
67	0.	0.
68	0.	0.

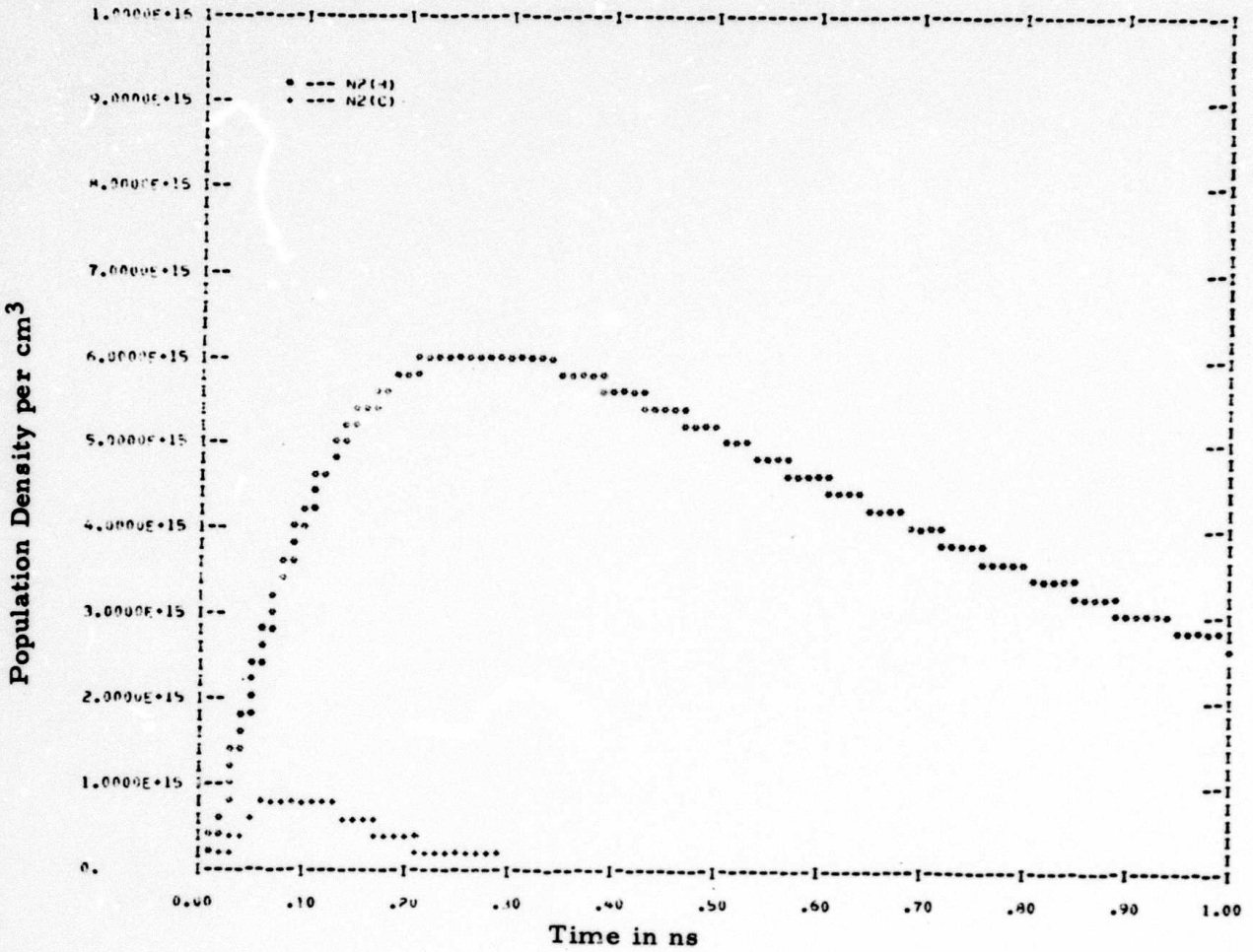

Figure 3. Population densities of $N_2(B)$ and $N_2(C)$ vs time due to excitation of 4 atm Ar + 5% N_2 by a 1.5 kA, 2 ns beam.

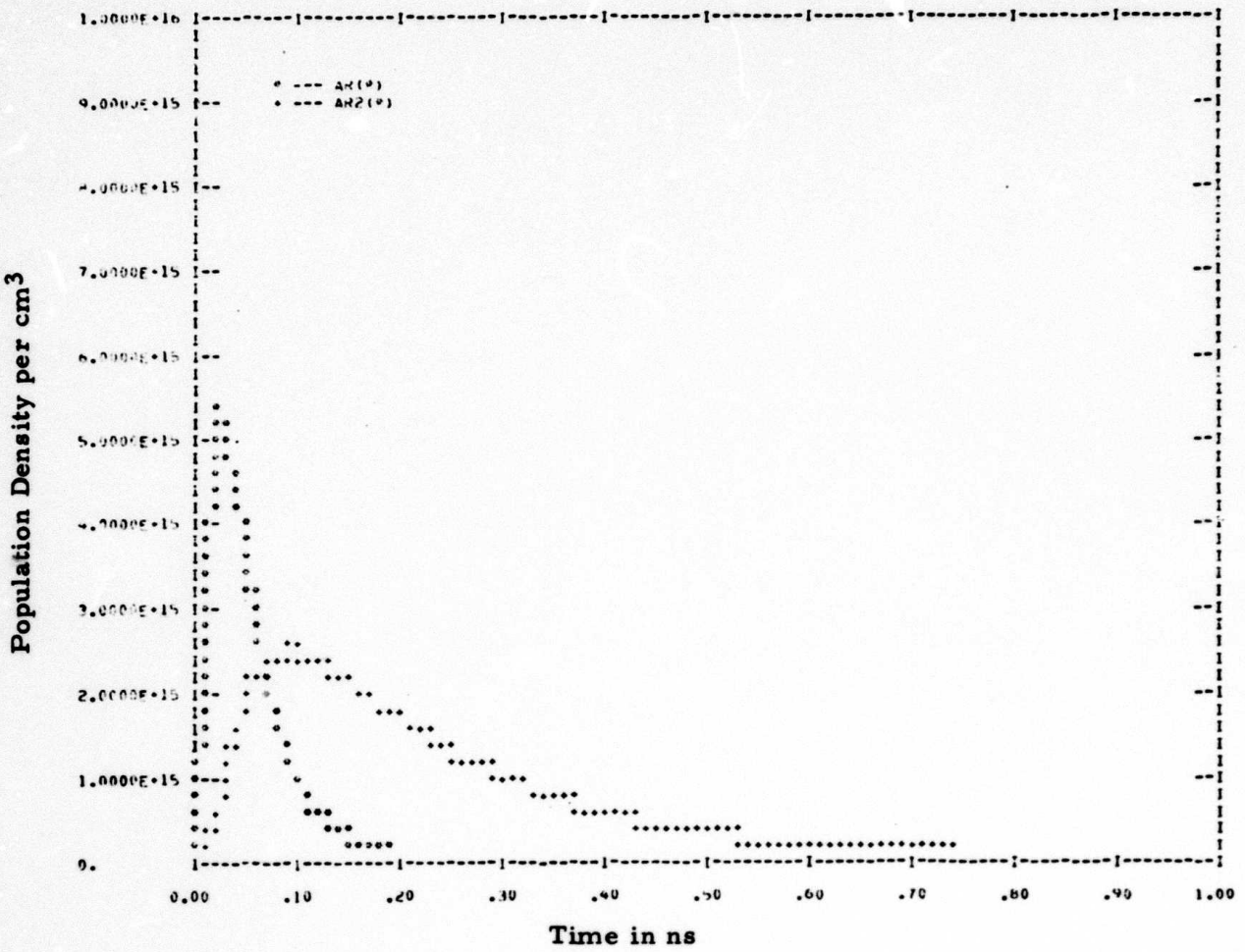

Figure 4. Population density of Ar^* and Ar_2^* vs time due to excitation of 4 atm Ar + 5% N_2 by a 1.5 kA, 2 ns beam.

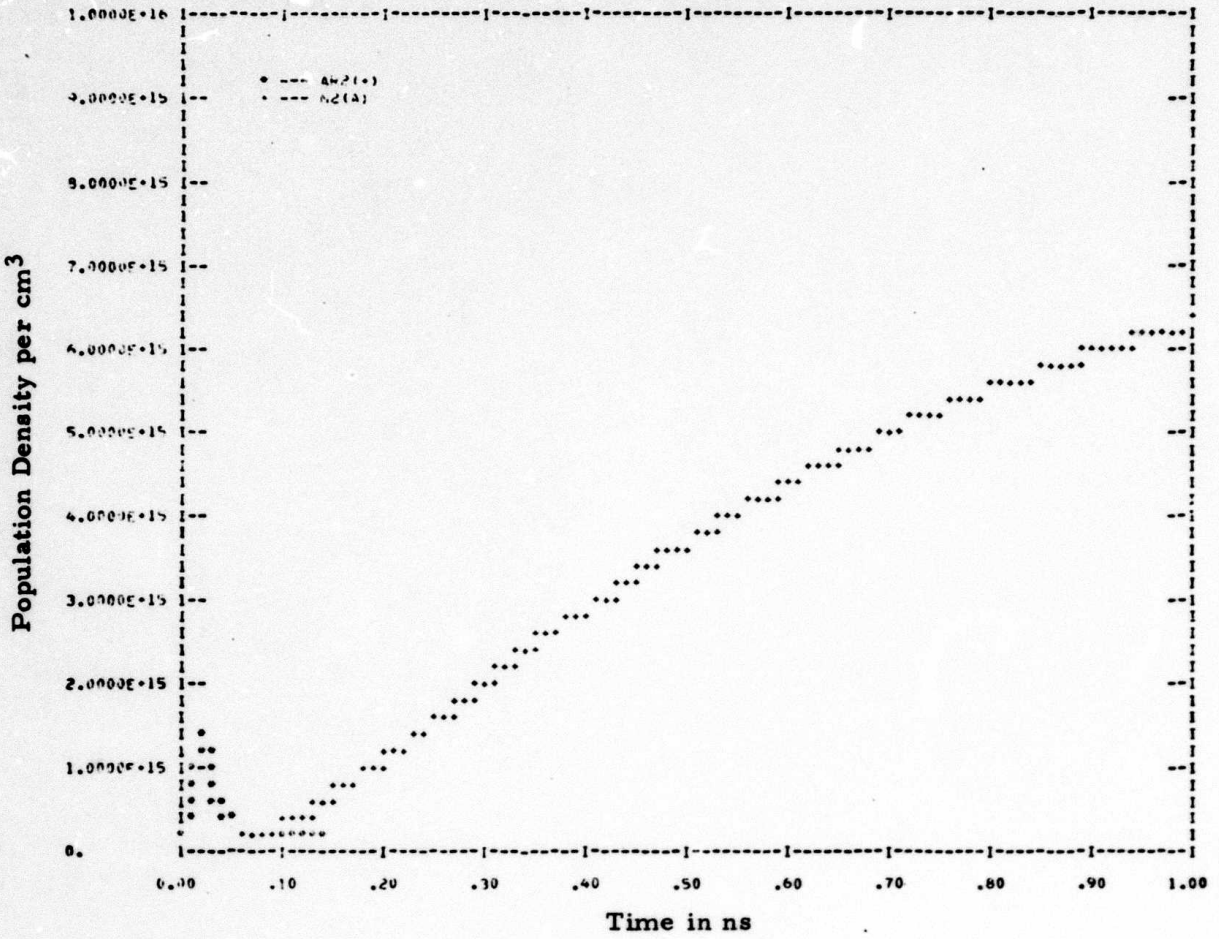

Figure 5. Population density of $N_2(A)$ vs time due to excitation of 4 atm Ar + 5% N_2 by a 1.5 kA, 2 ns beam.

model is being developed to predict the laser pulse shape, peak power, saturation intensity, extraction efficiency, etc.

The emphasis during the reporting period was placed on the calculations of the peak population efficiency under various conditions to get an indication of possible laser efficiencies. The peak population efficiency is defined by the ratio of the peak $N_2(C)$ population density to the time integrated density of excited Ar (both Ar^+ and Ar^*) created by the high energy E-beam pulse. A tentative laser efficiency was calculated on this basis and was defined by the total energy of the laser photons corresponding to the peak population density divided by the total energy expended in creating the initial Ar excitation.

The laser efficiency calculated on this basis for a 92 psia Ar and 8 psia N_2 excited by $400 A/cm^2$ in a 20 ns pulse was 0.22%. This efficiency agrees well with that observed experimentally under the same conditions and reported in the previous semiannual report NRTC 74-26R.

The principal reason for such a low efficiency seems to be quenching due to nonradiative losses from the laser upper level caused by the Ar and N_2 collisions. However, if the laser intracavity power is increased so that the rate of stimulated emission becomes higher than the rate of quenching, most of the upper state population may be extracted as radiation rather than losing it nonradiatively. The intracavity power may be increased by increasing the pump power and optimizing the output mirror coupling.

In the kinetic code, the successful competition by laser extraction against nonradiative losses are introduced by reducing the nonradiative quenching constant from $N_2(C)$. The results show that at 10 atm of Ar with 10% N_2 excited by 1 kA/cm^2, the efficiency can be as high as 2.5%. In experiments using the Pulserad 535, it was possible to obtain higher intracavity powers.

The results (described in Section 4) indeed show that a higher efficiency, ~2%, is achievable under these circumstances.

Finally, the highest laser efficiency predicted by the kinetic modeling was obtained from a mixture of 1 atm Ar with 5% N_2 excited by 1 kA beam. Some additive like He may have to be used to produce necessary cross relaxation. These studies indicate that an efficiency as high as 4.5% may be possible with the Ar-N_2 laser.

4.0 AR-N_2 LASER EXPERIMENTS

The Ar-N_2 transfer laser experiments, described in the previous semi-annual technical report, NRTC 74-26R, were carried out using the E-beam excitation facility, a Physics International Pulserad 110A. Parametric investigations of the Ar-N_2 laser were continued during this reporting period using the same facility. The main objective was to improve laser power and efficiency by optimizing both geometrical parameters as well as gas pressures and mixtures.

In the meantime, the installation of a much larger E-beam excitation facility was completed with necessary shielding and diagnostic equipment. This facility employs a Physics International E-beam gun, Pulserad 535, capable of delivering a 60 kA beam at 3 MeV in a 60 ns pulse, exceeding 10 kJ per pulse. The Ar-N_2 laser experiments are now being carried out using this new facility while the Pulserad 110A facility is being modified for the measurement of small signal gain coefficients.

4.1 Experiments with Pulserad 110A. Ar-N_2 experiments described previously utilized a 2.5 cm square cross section by 10 cm long gas cell. With 1 in. optics, this cell provided an optical volume of 30 cm^3. Two foils were used in these experiments. The first was a 3 mil titanium anode. This was followed by a 1 mil gas cell window which was supported by aluminum ribs (see Figure 6). The obvious disadvantage of this arrangement is the large scattering loss in the region between the foils. The mean scattering angle[5] $\bar{\theta}$ for 1 MeV electrons passing through a 3 mil titanium foil is 23°. The fraction of the beam which is not intercepted by the sides of the support ribs is further scattered by the gas cell window. Faraday cup measurements show that nearly half the beam is lost by the time it reaches the inside of the gas cell.

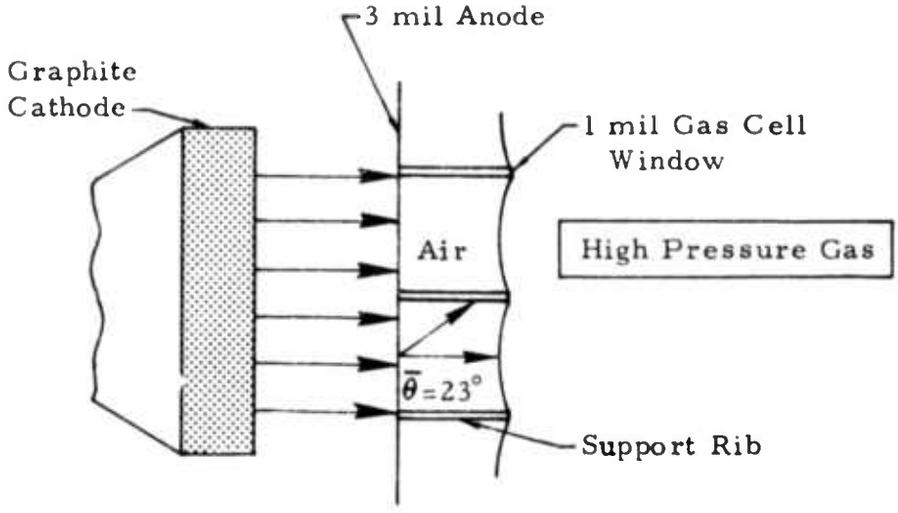

Figure 6. Double foil configuration.

Beam scatter occurring within the high pressure gas is unavoidable, but the beam loss described above can be reduced. By removing the anode foil and increasing the gas cell window thickness to 3 mil, nearly all the anode current enters the gas. In this configuration the support structure and the gas cell foil become the anode. Although the scattering angle remains the same, there is no drift region over which the beam can spread, therefore electrons enter the gas. This technique actually helps make the beam more uniform over the excited gas volume by removing small shadows cast by the foil support.

The laser was optimized for coupling, pressure and mixture in the single foil configuration. The energy output increased from the present value of 4 mJ to a new maximum of 12 mJ. Figure 7 shows the peak laser output power and energy as functions of the total pressure. These data are taken at the near optimum mixture of 9% obtained from inspection of the plot of output power vs mixture at constant pressure (Figure 8). The two curves peak at different pressures because the laser pulse becomes narrower at high pressures. At 150 psia the pulse width is approximately 10 ns. It is believed that nonradiative losses cause the output to decrease at higher pressures, even though the stopping power of the gas is increasing. To take advantage of higher pressure operation for the increased utilization of E-beam energy, the stimulated emission rate should be increased to compete with the quenching, as discussed in Section 3.

A second single foil gas cell was constructed with twice the gain length (20 cm) and twice the optical aperture diameter (2 inch). With the large aperture more of the electron beam can be absorbed by the gas before the beam is lost to the sidewalls of the gas cell. The present configuration was a 2 cm by 20 cm cathode which provides 500A/cm^2 at the gas/foil interface. However, with a narrower cathode (1 cm by 20 cm) a 1 kA/cm^2 beam can be used to excite half the cavity volume.

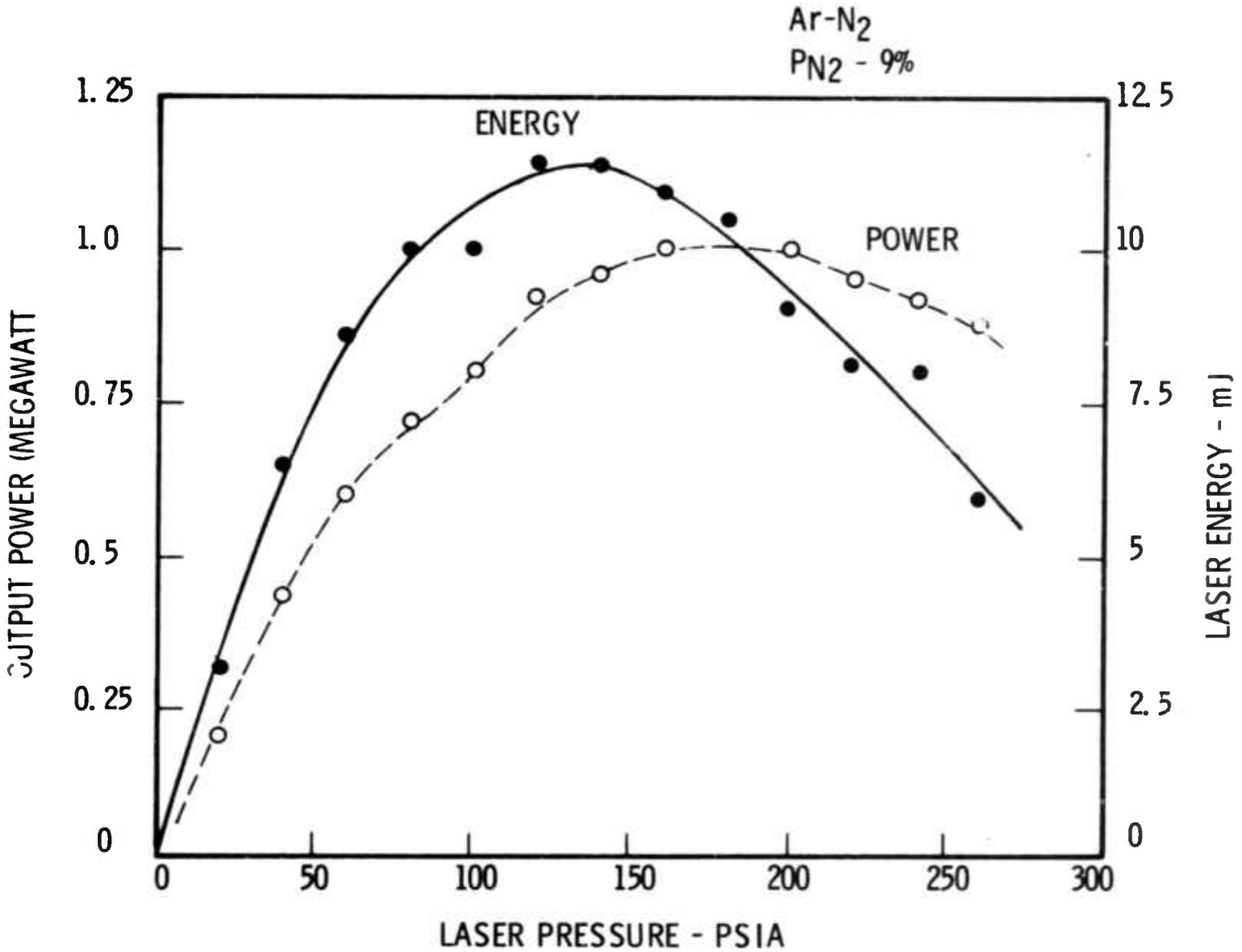

Figure 7. Output power and energy as a function of pressure

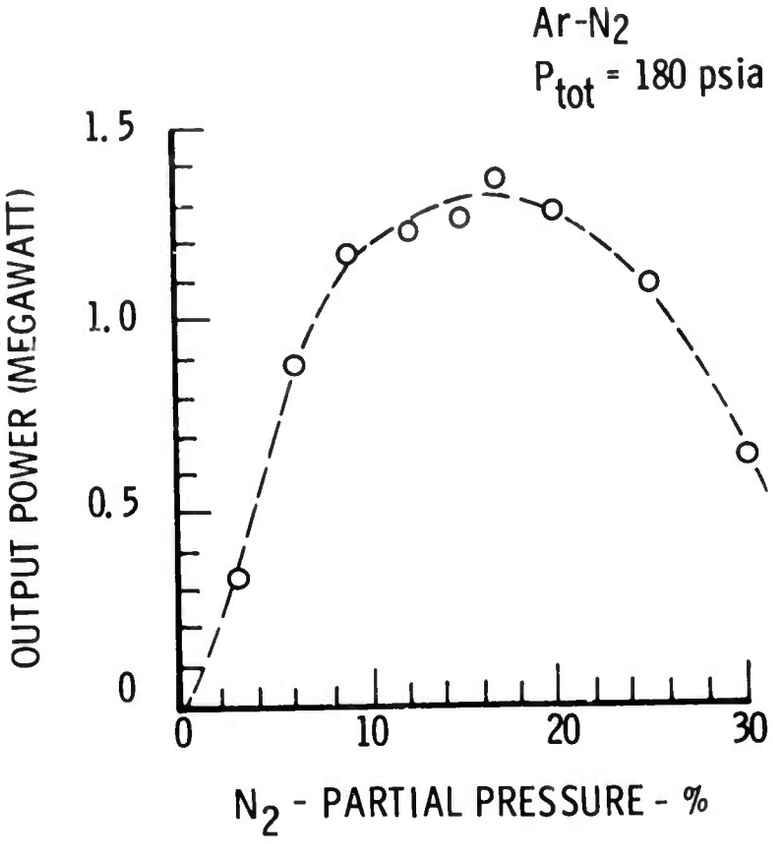

Figure 8. Output power as a function of mixture.

The initial experiments with $Ar-N_2$ showed similar pressure and mixture dependance observed before, but because of the more efficient use of the E-beam energy 20 mJ of laser energy was obtained at 3577Å. This corresponds to a peak power of approximately 2.5 MW. Figure 9 shows a typical laser pulse compared with the pulse obtained with the smaller 10 cm cavity. Because the round trip times are different, and a coupler with higher reflectivity was used with the 20 cm cavity (80% compared to 10%), the laser pulses exhibit different turn-on and decay characteristics.

The above data represents the optimum result obtainable with the Pulserad 110A. Since by this time the Pulserad 535 facility was available, further experiments on the $Ar-N_2$ laser were continued using the new facility.

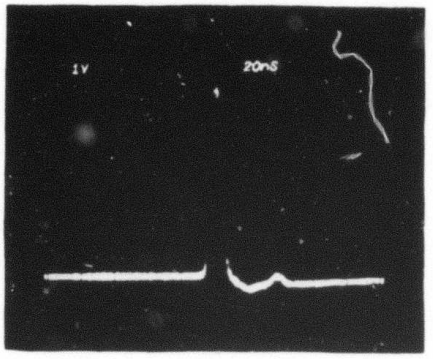

(a)

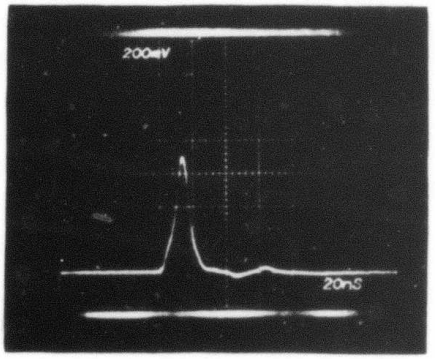

(b)

Figure 9. Ar-N_2 laser pulse for (a) 10 cm cavity at 1 kA/cm^2 and (b) 20 cm cavity at 500A/cm^2. Both shots taken with a 20% T coupler and a 10% mixture at 150 psia. Sweep 20 ns/cm. In (a) the peak power is ~0.5 MW; in (b) the peak power is ~2.5 MW.

4.2 Pulserad 535 Facility. The Pulserad 535 is a transmission line driven accelerator supplied to NRTC by DNA. This unique machine and its ancilliary equipment are specifically designed for laser research. With its 3 MeV energy, the beam can propagate without the need for an external magnetic field even at currents as large as 100 kA, with current densities of 3 kA/cm^2. Also, the scattering effects caused by foil windows and high pressure gases are much less pronounced at these energies. In addition, the foil window lifetime is greatly increased. The voltage and current pulses are nearly rectangular with fast rise and fall times ($\sim$10 ns). This insures a constant pumping rate for 50 ns. Figure 10 shows the cathode current and voltage for a typical shot.

Even though the amount of electromagnetic interference emitted by the Pulserad 535 is quite small, all diagnostic equipment is housed in a screen room. There are six simultaneous data acquisition channels, four with 150 MHz bandwidth and two with 500 MHz bandwidth. The final and essential component of the total facility is the extensive x-ray shielding, consisting of a 12 inch thick concrete ceiling and 24 inch thick concrete walls. Data may be taken at a rate limited only by the recycle time of the experiment and the requirement that the anode be changed about once in 30 shots. Hence, experimental programs can be carried out efficiently and rapidly in spite of the size and complexity of this type of laser excitation.

4.3 Experiments with Pulserad 535. Figure 11 shows a photograph of the Pulserad 535 experimental facility. The experimental arrangement is shown in Figure 12. For these measurements, a 10 cm long gas cell was used in a similar configuration as with the Pulserad 110A. However, the new cavity could accommodate either 1 inch or 2 inch diameter optics. Also, both aluminum and multilayer dielectric mirrors (prepared at Northrop) of different reflectivities were used.

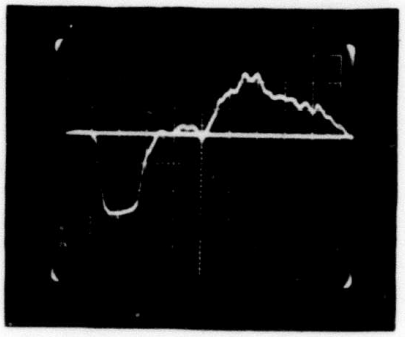

(a)

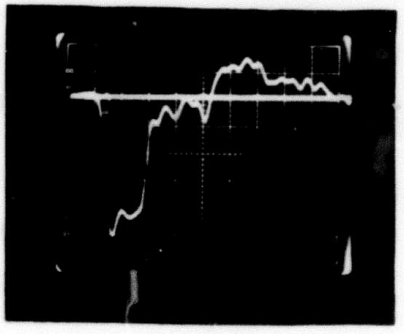

(b)

Figure 10. Pulserad 535 cathode current (a) and voltage (b). Horizontal scale 20 ns/div; vertical current scale ~ 30 kA/div; vertical voltage scale ~ 0.6 MeV/div.

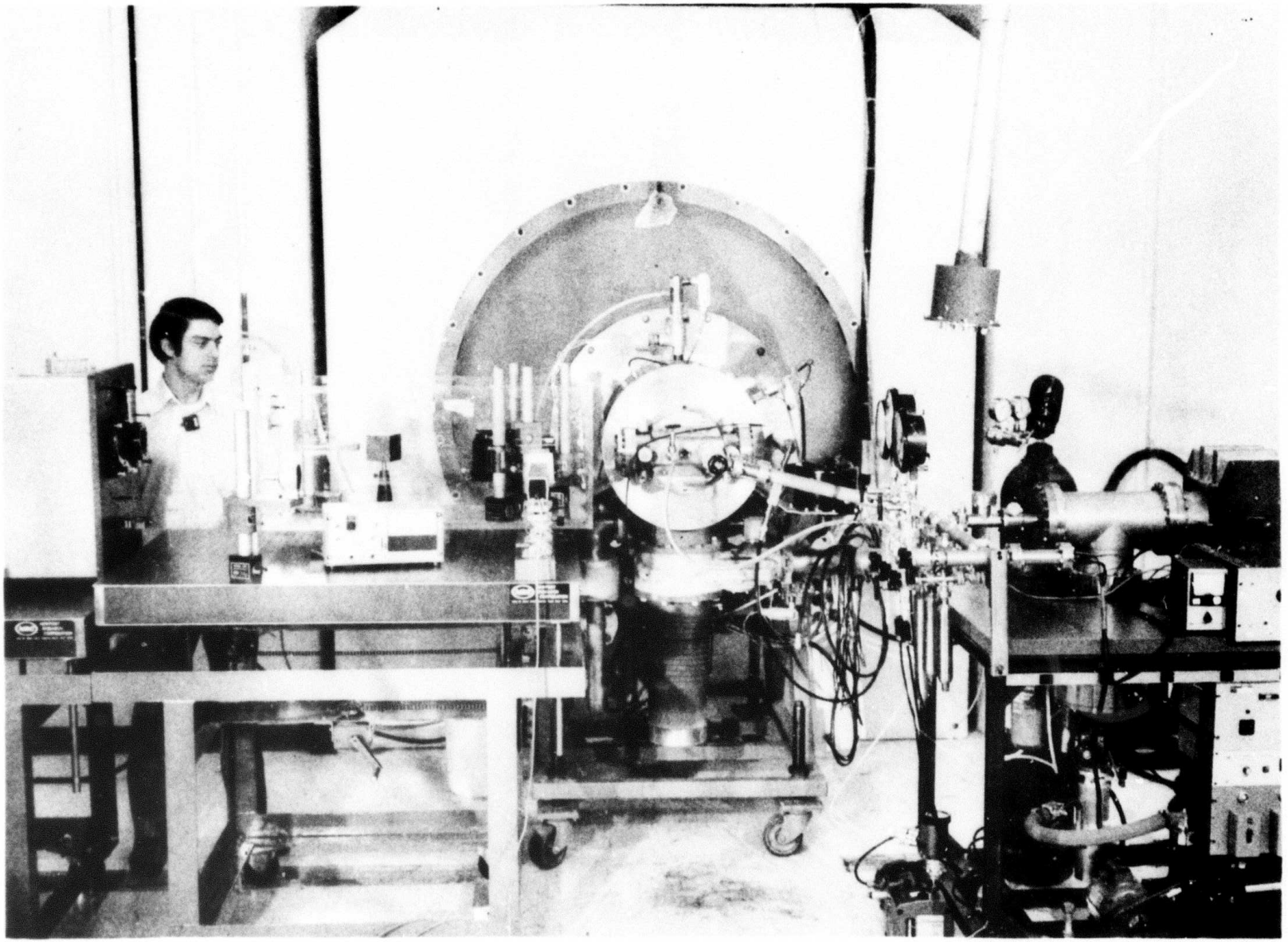

Figure 11. Photograph of the Pulserad 535 facility configured for Ar-N_2 transfer laser experiments.

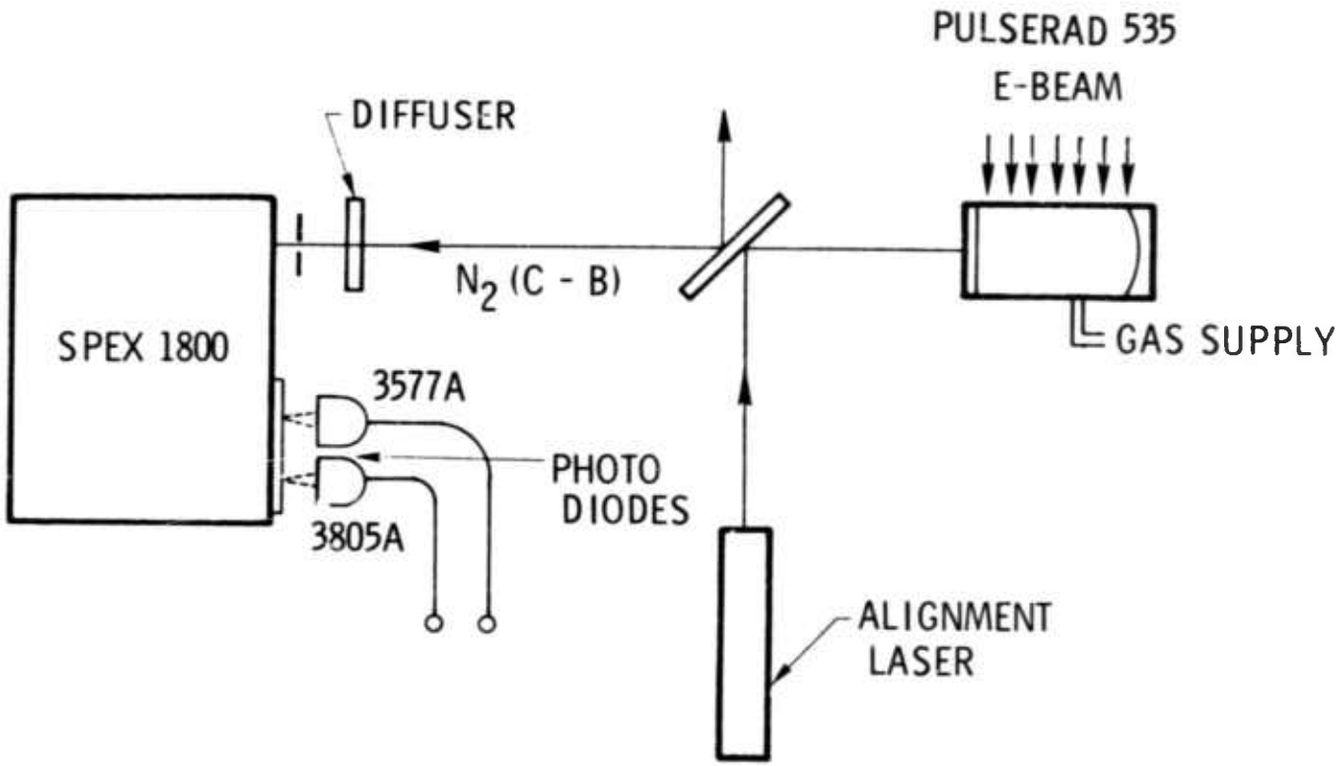

Figure 12. Experimental arrangement for the Ar-N_2 experiments using the 3 MeV E-beam.

Two series of experiments were conducted. In the first, basic parameters such as coupling, mixture and total pressure were varied to achieve the largest energy output and best efficiency. Using all dielectric optics, 230 mJ was obtained at 3577Å from a volume of 30 cm^3. This corresponds to a peak power of 11.5 MW for the 20 ns FWHM pulse. The efficiency with which the absorbed electron beam energy is converted to coupled out laser energy is estimated to be 2%. For these data the 82 kA beam (approximately 4 cm by 12 cm) was incident on a 3 cm by 10 cm gas cell foil window. Two foils were used, a 5 mil anode and a 3 mil gas cell window. With the same geometry and using foils one half as thick, Faraday cup measurements taken on the Pulserad 110A showed only one third of the beam current density appears at the optic axis of the high pressure gas. By using this reduction to estimate the current density in the Pulserad 535 experiments, and assuming the stopping power of the gas to be 33 keV/cm,[4] yields a pumping energy of 0.5J/cc, or an efficiency of 2%. Since careful timing measurements indicated the laser turned on in synchronism with the current pulse, the deposited energy was only calculated during the time corresponding to the FWHM of the laser pulse.

These experiments were extended to higher pressures (300 psia) where the laser pulse shortened to about 8 ns FWHM and increased in amplitude by more than a factor of 3. Further data could not be obtained because both the dielectric coupler and the aluminum total reflector were severely damaged by the high intensity laser radiation. We estimate that with the 80% reflective coupler, the circulating powers were in excess of 100 MW. Further study is under way to determine the peak power and output efficiency at pressures as high as 400 psia. So far, the major spectral component for this high intensity spike is the 0-1 band at 3577Å.

The second series of experiments was performed at pressures below 185 psia to prevent mirror damage. Here the objective was to study the temporal and spectral behavior of the Ar-N_2 system under the strong pumping of the

Pulserad 535 device. The 10 cm cavity was used with a 2 inch diameter all-dielectric optics. Careful attention was given to matching the cable delays of the two photodiodes and the Faraday cup to ±1 ns or better. The two photodiode amplitude responses are matched to 18% at 4000Å. Figure 13 shows the single shot spectra of a 10% N_2 mixture taken at 180 psia. The 0→1 and 0→2 transition bands are clearly visible. In Figure 14(a) the total C→B emission is displayed. When two photodiodes are used (refer to Figure 12), and one signal is delayed by 60 ns to separate the two spectral components, we see the 0-2 transition lases only after the 0-1 has turned off (Figure 14(b)). Figure 15 shows the timing sequence more clearly. The transition probability of the 0-1 band is about three times larger than that of the 0-2 band. Apparently the higher gain 0-1 line lases until the $B(v'' = 1)$ state fills up. Then the 0-2 lases until $B(v'' = 2)$ fills up, or the gain decreases due to lower pumping towards the end of the excitation pulse.

The occurrence of a relaxation oscillation is also indicated in the 3577Å radiation (Figure 14(a)). We believe the $N_2(C)$ level fills rapidly as the E-beam current enters the gas and the laser oscillations start readily until the gain is reduced by the increasing $N_2(B, v'' = 1)$ population. The first spike is seen to decay with about the cavity decay time, ~4 ns. When the laser recovers, the beam current has peaked so the second spike has increased amplitude. Then when the $N_2(B, v'' = 1)$ level is filled, the 0-2 line starts to oscillate.

4.4 Experiments with He Additive. From the potential energy diagram (Figure 2) and also from the kinetic modeling studies, it appears that nearly 30% of the excitation energy transferred to the $N_2(C)$ state is channeled through the $N_2(E)$ state or similar higher states.[6] Because of the meager data available in the literature on the relaxation rates from E→C, we performed a series of experiments to see if the addition of helium would affect a change in the laser's operating parameters. The Pulserad 110A with a 20 cm gain length cavity was selected. Helium was used both to alter the

Ar-N_2 LASER SPECTRUM

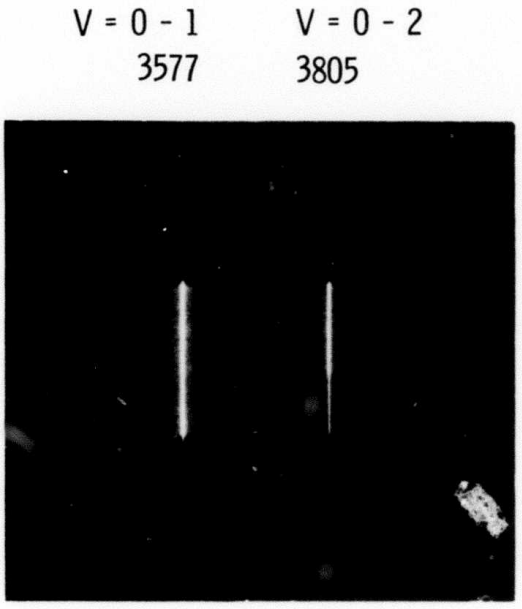

Figure 13. Ar-N_2 spectra showing the 0-1 and 0-2 bands. Total pressure 12 atm, 10% N_2.

TIME RESOLVED Ar-N_2 LASER SPECTRUM

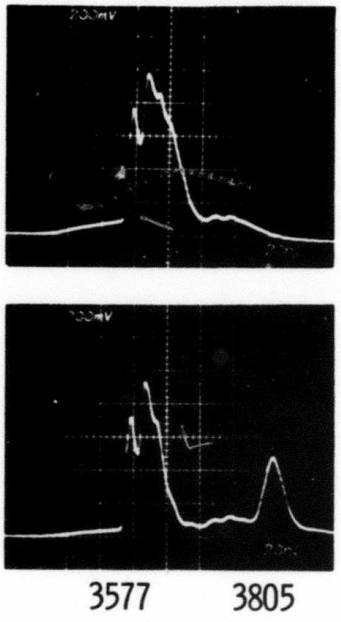

Figure 14. Ar-N_2 Laser pulses showing both 3577Å and 3805A lines simultaneously. (a) Total C→B emission; (b) 3805Å line delayed 60 ns to show separate time histories. 20% N_2 at 12 atm.

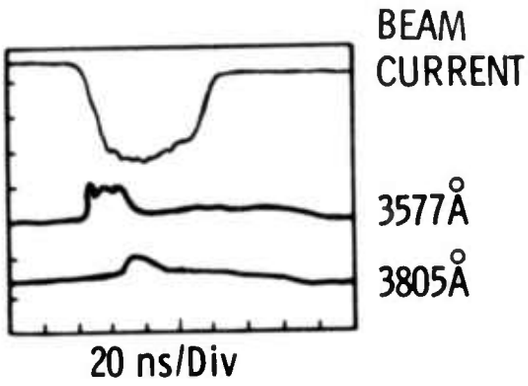

Figure 15. Timing diagram for Ar-N_2 Laser

Ar-N_2 mixtures and as an additive. In either case, the only change in peak laser power was the same as would be expected by the change in the stopping power of the gas mixture. Helium additions of 0 to 160% were used with 5%, 10%, and 20% mixtures of N_2 in argon. Figure 16 shows a typical plot of peak laser power vs the helium percentage in a mixture containing 10% N_2 in argon. The slight decrease in intensity nearly corresponds to the reduction in stopping power of the total gas mixture. This is borne out by the observation of a comparable increase in the transmission of the gas measured with the Faraday cup at the back of the gas cell. Therefore the helium had no decernable effect on the laser performance in these experiments.

There are three possible explanations for this negative result. First, the amount of excitation transferred to the $N_2(E)$ state may be smaller than we have assumed. Secondly, the $N_2(E) + He \rightarrow N_2(C)$ rate may be much smaller than we expect. The third and most likely explanation is that the kinetics is already dominated by the Ar-N_2 collisions and the addition of helium is not noticeable at these high pressures.

Two other experiments are planned to help clear up this point. A test made at even lower pressures would allow the kinetics to slow down so that the helium addition may give a positive result. These experiments were done with the Pulserad 110A which limited the pulsewidth to ~20 ns and no saturation effects were observed; repeating them at the same high pressures but with the longer 535 pulse may show a change in the relaxation oscillations or total pulsewidth, if He is able to relax the lower laser level more effectively.

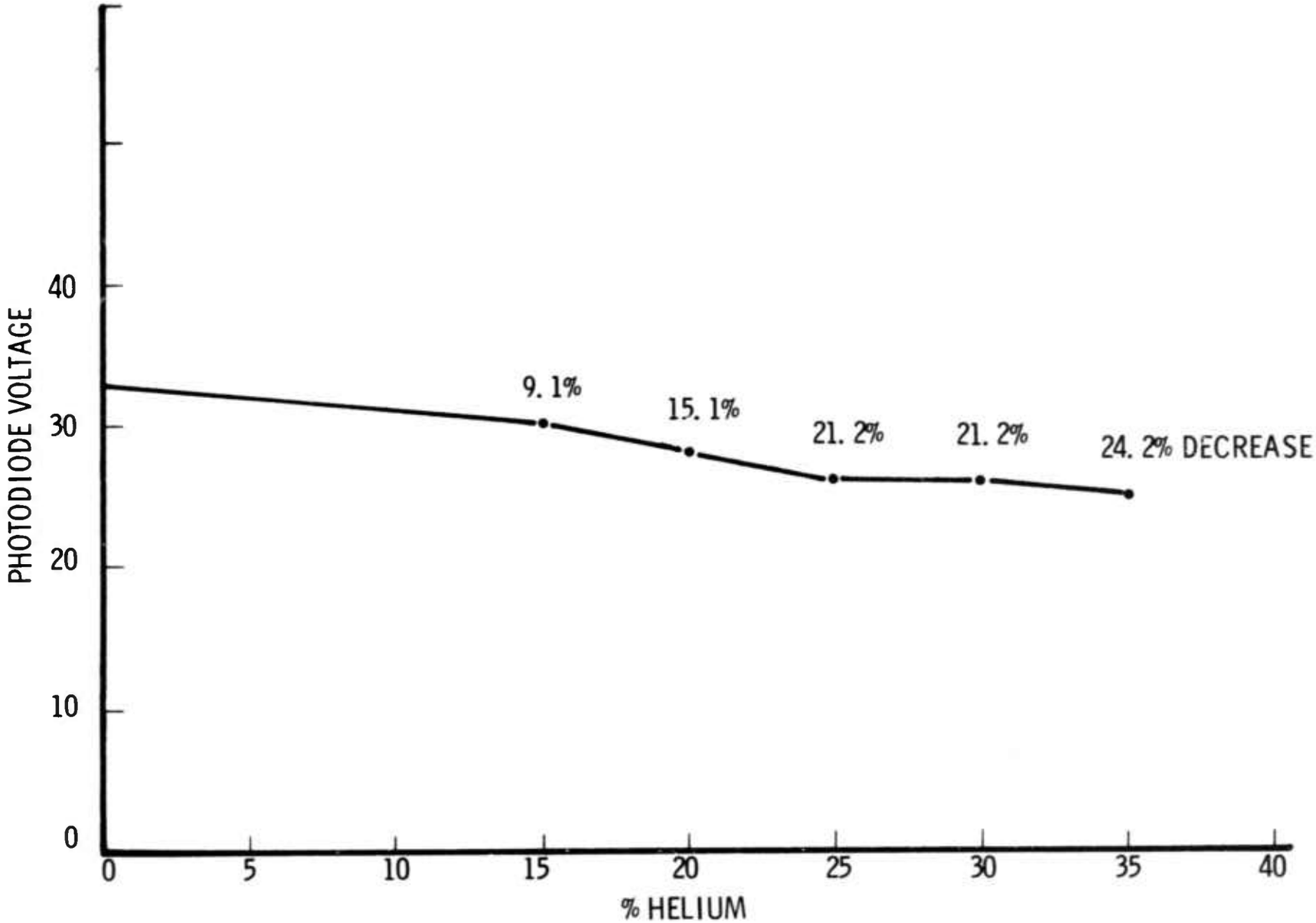

Figure 16. Pressure fixed at 60 psia total pressure - 10% Ar-N_2 mixture

5.0 REFERENCES

1. E. R. Ault, M. L. Bhaumik, W. M. Hughes, R. J. Jensen, C. P. Robinson, A. C. Kolb, and J. Shannon, IEEE, J. Q. E. 9, 1032 (1973); W. M. Hughes, J. Shannon, A. Kolb, E. Ault, and M. Bhaumik, Appl. Phys. Lett. 23, 385 (1973); W. M. Hughes, J. Shannon, R. Hunter, and A. Kolb, Paper Number Th A12, Optical Society of America meeting, Washington, D. C., 1974; W. M. Hughes, J. Shannon, and R. Hunter, Appl. Phys. Lett. 25, 85 (1974).

2. R. M. Hill, R. A. Gutcheck, D. L. Huestis, D. Mukherjee, and D. C. Lorents, Stanford Research Institute Report MP 74-39 (1974).

3. L. R. Peterson and J. E. Allen, J. Chem. Phys. 56, 6068 (1972).

4. M. J. Berger and S. M. Seltzer, National Academy of Science Report 1133 (1964).

5. V. F. Baranov and O. A. Pavlovskii, Atomnaya Énergiya 25, 317 (1968).

6. R. M. Hill and D. C. Lorents, Stanford Research Institute, (private communciation).

ACKNOWLEDGMENT

The efforts of Dr. W. B. Lacina in developing the kinetics computer code are deeply appreciated. Also the invaluable assistance of C. F. Zahnow and D. D. Floyd in setting up and operating the experiments is gratefully acknowledged.